IEEE Access
Multidisciplinary | Rapid Review | Open Access Journal

Received February 28, 2020, accepted March 11, 2020, date of publication March 20, 2020, date of current version March 31, 2020.

Digital Object Identifier 10.1109/ACCESS.2020.2982259

Solar Position Acquisition Method for Polarized Light Navigation Based on ∞ Characteristic Model of Polarized Skylight Pattern

BIANBIAN LIU, ZHIGUO FAN, (Member, IEEE), AND XIANQIU WANG
Key Laboratory of Knowledge Engineering with Big Data (Hefei University of Technology), Ministry of Education, Hefei 230601, China
School of Computer Science and Information Engineering, Hefei University of Technology, Hefei 230601, China

Corresponding author: Zhiguo Fan (fzg@hfut.edu.cn)

This work was supported by the National Natural Science Foundation of China under Grant 61571177.

ABSTRACT Inspired by the use of polarized information for navigation behaviors in nature, many researchers have carried out a lot of researches on bionic polarized light navigation. Due to the complexity of the atmospheric radiation transmission process, there is a lot of uncertainty for the bionic polarized light navigation method that accurately calculates the polarization information of the polarized skylight pattern pixel by pixel. This paper studies the distribution of the polarized skylight pattern under different weather conditions through a large number of observational experiments. It is found that the distribution of the angle of polarization shows a stable ∞ characteristic, which can reflect the macro distribution characteristics and changing laws of the polarized skylight pattern. This paper extracts the ∞ characteristic from the polarization angle image, then we establish a model of ∞ characteristic to solve the solar position by calculating the feature similarity indexes between the measured ∞ characteristic images and Rayleigh ∞ characteristic images. And we propose an improved harmony search algorithm to solve the optimal solution of the model. By searching in the Rayleigh ∞ characteristic image database, the solution vector corresponding to the Rayleigh ∞ characteristic image with the highest feature similarity index is the solar position. In this paper, experiments are performed on measured polarized images under sunny and cloudy weather, and the experimental results verify the effectiveness of the proposed algorithm.

INDEX TERMS Polarized light navigation, solar position, polarized skylight pattern, harmony search algorithm, Rayleigh model.

I. INTRODUCTION

Sunlight is natural light without polarization.When it passes through the atmosphere and scatters with atmospheric molecules, aerosol particles, etc., it forms the polarized skylight pattern [1]–[5]. There is a lot of evidence that many animals in nature are sensitive to the linear polarization of light and have the ability to sense the direction of the E-vector of the polarized skylight pattern [6], [7]. For example, after Cataglyphis ants travel hundreds of meters looking for food, they can return to their nests along an approximately straight path. Wehner, Switzerland, studied the navigation behavior of Cataglyphis ants and found that they use polarized skylight pattern to navigate, relying on their compound eyes that are highly sensitive to polarization [8]. Australian C. Evangelista experimentally demonstrated that flying bees can get navigation information purely from polarized light, and communicate this information to their nest-mates through 'waggle dance' [9]. Bats are the only mammal known so far to make use of the polarized skylight pattern. Greif *et al*. from the United Kingdom demonstrated that the femal mouse-eared bat (Myotis myotis) uses polarization information at sunset to correct the magnetic compass, which is subsequently used for orientation during a homing experiment [10].

Inspired by the use of polarized information for navigation behaviors in nature, many researchers have carried out a series of studies on bionic polarized light navigation and found that the polarized skylight pattern has some macro distribution laws [1], [2], [11]. In bionic polarized light navigation, there are two main ways to obtain navigation

The associate editor coordinating the review of this manuscript and approving it for publication was Emre Koyuncu.

information using the polarized skylight pattern. One is to obtain the azimuth information of the carrier by obtaining the angle information of the solar meridian. The other is to first obtain the solar position information, that is, the solar zenith angle and azimuth, and then the latitude and longitude information is inverted from the position of the sun to complete the location of the carrier [12], and the azimuth information of the carrier can also be obtained. For example, the solar meridian has three features, namely the E-vector of 90 °, a straight line, and passing through the principal point. Lu *et al.* use this rule to propose an orientation algorithm. The algorithm first obtains the binary image of the solar meridian through threshold extraction, and then transform the binary points into the parameter space by Hough transform. The peak in the parameter space stands for the solar meridian, whose coordinates are the parameter of the solar meridian [13], [14]. In addition, the polarized skylight pattern under different sky conditions has been studied through polarization imaging measurement. It is found that the symmetry of the AOP image is very stable under most sky conditions [15]. Zhao *et al.* use this feature to propose a polarized navigation method by scanning of symmetry axis and curve fitting. First, degree of polarization mapping is used to exclude invalid data, and 1000 pairs of pixels are randomly selected in one calculation. The optimal solar azimuth estimation can be obtained by searching for different symmetry values. Finally, curve fitting is applied to the data generated by dense scans to obtain the best estimate of the solar meridian [16]. Also, according to the Rayleigh single-scattering model, the E-vector of scattered light is perpendicular to the scattering plane [17]. He *et al.* present an unsupervised method for polarization navigation when the sky is partly blocked. Based on the solar meridian vector perpendicular to the E-vector, they design a rule to extract the pixels of sky region according to the Rayleigh single-scattering model, and after extracting the sky region, the pixels in the sky region are used to accurately calculate the azimuth [18].

The above macro distribution laws are based on the Rayleigh single-scattering model, but it is obvious that the atmospheric radiation transmission process is a fairly complex multiple scattering process, and the types and distribution of particles in the atmosphere are non-uniform, so the actual polarized skylight pattern does not exactly follow the Rayleigh single-scattering model. Through a large number of observational experiments, we found that the distribution of the angle of polarization of the polarized skylight pattern presents a stable ∞ characteristic, and ∞ characteristic always exists stably under sunny, foggy, and cloudy weather conditions [19], [20]. The representation equation of the ∞ characteristic is an analytical function which describes the point set with the same direction of the E-vector of the polarized skylight pattern [21], and it is the only significant feature in the distribution of the polarized skylight pattern found so far that meets the requirements of stability, uniqueness, measurability, and resolvability [5], which reflects the macroscopic distribution characteristics and changing rules of the polarized skylight pattern.

Aiming at the ∞ distribution characteristics of the polarized skylight pattern, this paper proposes a method based on the improved harmony search (IHS) algorithm to solve the position of the sun by using the polarized skylight pattern. Firstly, we extract ∞ characteristic of the polarized skylight pattern from the polarization angle image, and then calculate the feature similarity (FSIM) index between the measured ∞ characteristic image and Rayleigh ∞ characteristic image. Thus a ∞ characteristic model can be established to solve the solar position. And we propose an improved harmony search algorithm to solve the optimal solution of the model. In order to improve the search efficiency, two initializations of the harmony memory are designed. By searching in the Rayleigh ∞ characteristic image database, we get the Rayleigh ∞ characteristic image with the highest feature similarity index, and the corresponding solution vector is used as the solar position.

II. CHARACTERISTIC MODEL OF SOLAR POSITION

A. ∞ CHARACTERISTIC MODEL OF POLARIZED SKYLIGHT PATTERN

Polarized skylight pattern is a special polarization state distribution formed by polarized light due to atmospheric scattering, radiation, and absorption during the transmission of sunlight in the atmosphere. It is one of the important natural attributes of the earth [5]. Rayleigh single-scattering model is a classic method to describe polarized skylight pattern, which can accurately characterize the distribution characteristics of polarized skylight pattern in an ideal atmospheric environment. It can be described by the degree of polarization (DOP) and angle of polarization (AOP). As shown in Fig.1, the Rayleigh representation model coordinate system of the polarized skylight pattern is established with the observer as the origin O, the positive east direction as the X axis, the positive north direction as the Y axis, and the vertical line passing through the zenith as the Z axis. The zenith angle of any point $P(r, \theta, \varphi)$ on the sphere is θ, the azimuth angle is φ and starts from the north direction, and the north-east direction is positive. The spatial position of the sun is expressed as $S(r, \theta_s, \varphi_s)$, where θ_s is the solar zenith angle, φ_s is the solar azimuth angle.

The angle between the observed point P and the sun S is called the scattering angle γ , and the degree of linear polarization at this point can be expressed as:

$$P = P_{\max} \sin^2 \gamma \Big/ \left(1 + \cos^2 \gamma\right) \tag{1}$$

where $P_{\max}$ represents the maximum degree of polarization (theoretical value is 1).

The angle α between the E-vector at the measured point P and the local meridian at the point is defined as the angle of polarization at the point. The distribution of angle of polarization is the point set with the same direction of the

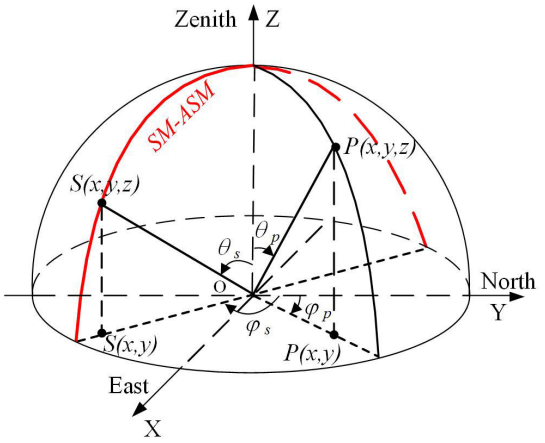

FIGURE 1. Rayleigh representation model coordinate system of the polarized skylight pattern.

E-vector of the polarized skylight pattern. According to the Rayleigh single-scattering model, it can be described as:

$$\tan\alpha = \frac{\sin\theta\cos\theta_s - \cos\theta\cos(\varphi-\varphi_s)\sin\theta_s}{\sin(\varphi-\varphi_s)\sin\theta_s} \tag{2}$$

Let the radius of the celestial sphere $r = 1$, the transformation relationship between the coordinates (r, θ, φ) of any point in the spherical coordinate system and its coordinates (x, y, z) in the three-dimensional Cartesian coordinate system is expressed as:

$$\begin{cases} x = \sin\theta\cos\varphi \\ y = \sin\theta\sin\varphi \\ z = \cos\theta \end{cases} \tag{3}$$

By introducing (3) into (2) and simplifying it, the three-dimensional representation equation of the point set with the same direction of the E-vector of the polarized skylight pattern [21] is shown in equation (4).

$$\begin{cases} \sqrt{1-x^2-y^2} - z = 0 \\ (x\sin\varphi_s - y\cos\varphi_s)\sin\theta_s\tan\alpha + \left(x^2+y^2\right)\cos\theta_s \\ \quad -\sqrt{1-x^2-y^2}\,(x\cos\varphi_s + y\sin\varphi_s)\sin\theta_s = 0 \end{cases} \tag{4}$$

In order to facilitate the analysis of the polarized skylight pattern, the three-dimensional distribution pattern is vertically projected to the ground level, and a two-dimensional projection representation of the point set with the same direction of the E-vector of the polarized skylight pattern in equation (5) can be obtained, that is, ∞ characteristic model of the polarized skylight pattern.

$$\begin{aligned} &(x\sin\varphi_s - y\cos\varphi_s)\sin\theta_s\tan\alpha + \left(x^2+y^2\right)\cos\theta_s \\ &\quad -\sqrt{1-x^2-y^2}\,(x\cos\varphi_s + y\sin\varphi_s)\sin\theta_s = 0 \end{aligned} \tag{5}$$

Fig.2 shows a comparison between the Rayleigh single-scattering model and the ∞ characteristic model. It can be seen from the fig.2 that the two have similar morphological

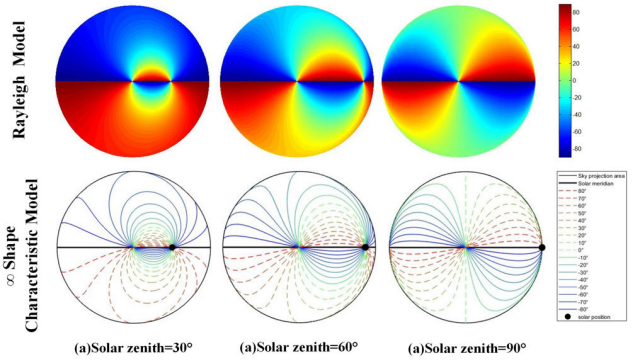

FIGURE 2. The comparison between the Rayleigh single-scattering model and the ∞ characteristic model.

distribution characteristics, and the change trend of the two also remains consistent as the solar zenith angle increases.

However, due to the multiple scattering of particles at different scales in the atmosphere and the effects of polarization singularities [22], the measured polarized skylight pattern does not fully follow the Rayleigh single-scattering model. In order to study the distribution of Rayleigh points in the AOP images, a quantitative analysis was performed [2].

Using the measured polarization angle image at a given solar position, we calculate the angle of polarization difference $\Delta\alpha = \left|\alpha_{mear} - \alpha_{Rayleigh}\right|$ at every celestial point between the real sky and Rayleigh single-scattering sky, where α_{mear} represents the measured polarization angle image and $\alpha_{Rayleigh}$ represents the Rayleigh single-scattering simulated polarization angle image. When the angle of polarization difference of a point is $\Delta\alpha \leq \alpha_{thres}$, this point is called "Rayleigh" point, otherwise it is called "non-Rayleigh" point. We introduce the proportion k of the sky that follows the Rayleigh model, the definition of which is $k = N_{Rayleigh}/N$. Then the Rayleigh points of those celestial points are counted for the number $N_{Rayleigh}$, and N is the total number of pixels in the circular picture of the sky.

In this paper, the threshold α_{thres} is set to 5°, and the Rayleigh point distribution under sunny weather is shown in Fig.3. By comparing with the corresponding AOP images, it can be clearly seen that the proportions of Rayleigh points

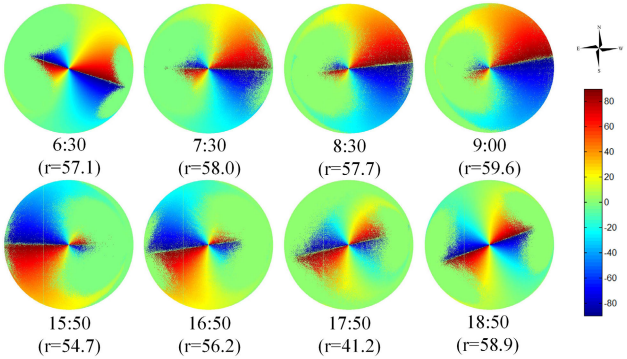

FIGURE 3. The distribution of Rayleigh points under sunny weather.

under sunny weather are between 40% and 60%, and the distribution of Rayleigh points meets the ∞ characteristic.

From Fig.3, we can know that the proportion of non-Rayleigh points in the AOP images even under sunny weather is still very large, which indicates that a considerable part of the data is not consistent with the Rayleigh single-scattering model. Therefore, if the Rayleigh single-scattering model is used to process the measured polarization image, a large error will occur in the result, and the amount of data processed will be large. Therefore, this paper samples the data from the polarization angle image and extracts the stable ∞ characteristic as the characteristic model of this paper. From the current research results, for an unknown polarization image, we cannot distinguish whether the data in it are Rayleigh point or non-Rayleigh point. But by analyzing the distribution of Rayleigh points under sunny and cloudy weather in a long time, we find that data with angles of polarization less than 20° in polarized images mainly belong to the non-Rayleigh points, and the Rayleigh points are evenly distributed in the range of $20° \leq |\alpha| \leq 90°$. At the same time, in order to reduce the amount of calculation, we select the points in the AOP image whose angle of polarization values are in the range of $R + 1°$, where R is an array with 10° interval in the range of $20° \leq |\alpha| \leq 90°$. To sum up, this paper chooses a total of 16 groups of ∞ characteristic to form ∞ characteristic models.

B. SOLAR POSITION SOLVING MODEL

In order to obtain the solar position from the polarization angle image without solar position information, this paper builds a solar position solving model based on the ∞ characteristic model. The principle of this model is to find the optimal characteristic image obtained from the polarized skylight pattern ∞ characteristic model database. The optimal characteristic image best matches the measured ∞ characteristic image, thereby we can achieve the estimation of the solar position through the optimal characteristic image.

It can be known from equation (5) that the polarization angle image $AOP(p_i) = AOP(\theta_i, \varphi_i)$ with known solar position can be generated by ∞ characteristic model of the polarized skylight pattern. The goal of this paper is to find the position of the sun from an unknown polarization angle image $AOP(\theta_x, \varphi_x) = AOP(p_x)$. In order to establish the relationship between $AOP(p_i)$ and $AOP(p_x)$, the two images are first sampled to obtain the corresponding ∞ characteristic image $Eight(p_i)$ and $Eight(p_x)$, where the data value of the ∞ characteristic region is 1 and the data value of the non-∞ characteristic region is 0.

$$Eight(x, y) = \begin{cases} 1, & 20° \leq |\alpha| \leq 90° \\ 0, & else \end{cases} \tag{6}$$

In equation (6), $Eight(x, y)$ shows the value of a point (x, y) on the ∞ characteristic image $Eight(p_i)$, where $Eight(x, y) = 1$ indicates that the point belongs to the ∞ characteristic region, and $Eight(x, y) = 0$ indicates that the point belongs to the non-∞ characteristic region.

The feature similarity (FSIM) index [23] is then used to calculate the similarity between the ∞ characteristic images $Eight(p_i)$ and $Eight(p_x)$. The computation of FSIM index consists of two steps. In the first step, the local similarity map $S_L(x, y)$ is computed, and then in the second step, we pool the similarity map into a single similarity score FSIM.

$$S_L(x, y) = S_{PC}(x, y) \cdot S_G(x, y) \tag{7}$$

Among them, $S_{PC}(x, y)$ and $S_G(x, y)$ respectively represent the phase congruency (PC) similarity and gradient magnitude (GM) similarity of the two ∞ characteristic images. PC is used as the primary feature in computing FSIM. Meanwhile, considering that PC is contrast invariant, but image local contrast does affect human visual system' perception on the image quality, the image GM is computed as the secondary feature to encode contrast information. PC and GM are complementary and they reflect different aspects of the human visual system in assessing the local quality of the ∞ characteristic images. Having obtained the similarity $S_L(x)$ at each location x, the overall similarity between the two ∞ characteristic images can be calculated. However, different locations have different contributions to human visual system' perception of the image. Therefore, we use $PC_m = \max(PC_1(x), PC_2(x))$ to weight the importance of $S_L(x)$ in the overall similarity between the two ∞ characteristic images, and accordingly, the FSIM index between the two ∞ characteristic images is defined as follows:

$$FSIM = \frac{\sum_{(x,y)\in\Omega} S_L(x, y) \cdot PC_m(x, y)}{\sum_{(x,y)\in\Omega} PC_m(x, y)} \tag{8}$$

where Ω means the whole image spatial domain.

In the ∞ characteristic model database based on the Rayleigh single-scattering model, we find the characteristic image with the highest similarity to the ∞ characteristic of the unknown solar position image. That is, we need to find the maximum value of FSIM, and then we can get the solar position p_c of the image.

$$p_c = \arg\max(FSIM(p_x, p_i)), \quad i = 1, 2, \ldots, n \tag{9}$$

III. SOLAR POSITION SOLVING ALGORITHM

We design an improved harmony search algorithm to search the characteristic image with the largest FSIM in the Rayleigh ∞ characteristic image database. Because the initial search range is very large, in order to improve the search efficiency, we design to initialize the harmony memory twice: sparse initialization of harmony memory HM1 and dense initialization of harmony memory HM2. The angle range for sparse initialization is $0° \leq \theta_i \leq 90°, 0° \leq \varphi_i \leq 360°$, with 5° as the step size. The initial position of the sun is determined by sparse initialization. Dense initialization will be performed around the initially determined solar position, in steps of 1°. After the dense initialization is completed, HM2 is updated 1000 times, and the solution vector

corresponding to the minimum value of the negative FSIM is the optimal solar position.

Harmony search (HS) is a new meta-heuristic algorithm developed by Geem *et al*. [24], which is inspired by the natural musical performance process that occurs when a musician searches for a better state of harmony. In the HS algorithm, the solution vector is analogous to the harmony in music, and the local and global search schemes are analogous to musician's improvisations. It was evolved by the idea that musicians relied on the adjustment of the pitch of each instrument to achieve a wonderful harmony state. In music performance, the best state is determined by aesthetic estimation, which is determined by the set of sounds played by the combined instrument, just as the objective function evaluation is determined by the set of values generated by variables. Exercises can produce sounds that improve aesthetic evaluations, just as iterative searches can improve the value of better objective function evaluations. This paper adopts an improved harmony search (IHS) algorithm and applies it to the above-mentioned solar position solving model, which not only improves calculation efficiency, but also improves the accuracy of the solution.

The basic HS algorithm consists of three basic steps, namely, initialization, improvisation of a harmony vector and updating the HM. In the basic HS algorithm, each solution is called a "harmony" and represented by an n-dimension real vector. An initial population of harmony vectors are randomly generated and stored in a harmony memory (HM). Then a new candidate harmony is generated from all of the solutions in the HM by using a memory consideration rule, a pitch adjustment rule and a random re-initialization [25]. Finally, the HM is updated by comparing the new candidate harmony and the worst harmony vector in the HM. The worst harmony vector is replaced by the new candidate vector if it is better than the worst harmony vector in the HM. The above process is repeated until a certain termination criterion is met.

Applying the HS algorithm to the above solution model, the harmony of each instrument corresponds to the solution vector $p_i = (\theta_i, \varphi_i)$, where the evaluation index is expressed by the feature similarity index $FSIM\ (p_x, p_i)$, where $p_x = (\theta_x, \varphi_x)$ represents the solar position parameter in the unknown ∞ characteristic image. The harmony vectors and its evaluation results are stored in the harmony memory, as shown in equation (10), and the composition process is the search process of the optimal solution.

$$HM = \begin{bmatrix} p_1 \\ p_2 \\ \vdots \\ p_n \end{bmatrix} = \left[\begin{array}{cc|c} \theta_1 & \varphi_1 & -FSIM\ (p_1) \\ \theta_2 & \varphi_2 & -FSIM\ (p_2) \\ \vdots & \vdots & \vdots \\ \theta_n & \varphi_n & -FSIM\ (p_n) \end{array}\right] \quad (10)$$

In order to verify the correctness of the algorithm proposed in this paper, experiments are performed on a set of Rayleigh polarized images with the solar position (45°, 180°). In order to traverse all possible positions of the sun, the harmony memory is initialized within the effective range of the solar

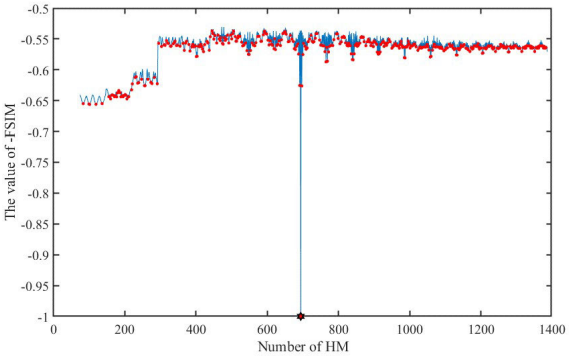

FIGURE 4. Rayleigh polarized image experimental results for the solar position (45°, 180°).

zenith and azimuth in steps of 5°, and the maximum iteration is set to 0. The algorithm model in this paper is used to process the Rayleigh polarization image with (45°, 180°) as the solar position. The experimental results are shown in Fig.4.

In Fig.4, the abscissa represents the serial number i of the possible solar position in the harmony memory, and the ordinate represents the $-FSIM\ (p_x, p_i)$ value of the solar position p_i in harmony memory. The red dot in Fig.4 indicates the position of the minimal value appearing in the curve, and the minimum value is marked with a hexagonal star. The position of the sun corresponding to the position of the minimum value in Fig.4 is (45°, 180°), which is in line with expectations and verifies the effectiveness of the algorithm in this paper. In order to study the changing law of the FSIM value with the movement of the sun, the following experiments are designed. The first step: the solar zenith angle is set to 45°, traverse the solar azimuth from 0° to 360° in steps of 1°. The experimental results are shown in Figure 5 (a); the second step: the solar azimuth is set to 180°, traverse the solar zenith from 0° to 90° in steps of 1°. The experimental results are shown in Figure 5 (b).

As can be seen from Fig.5 (a), the optimal azimuth is 180°, and the curve is roughly symmetrical with a straight line perpendicular to the optimal azimuth, the negative FSIM value gradually increases in the form of waves as it is far away from the optimal azimuth, that is, the similarity is getting lower, which is in line with our expectations. The optimal zenith angle in Fig.5 (b) is 45°. Similarly, the negative FSIM value gradually increases as it is far away from the optimal

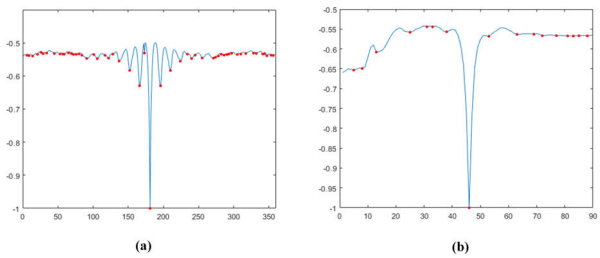

FIGURE 5. Experimental results. (a). Search results with zenith angle of 45° and azimuth of 0° to 360°. (b). Search results with azimuth of 180° and zenith angle of 0° to 90°.

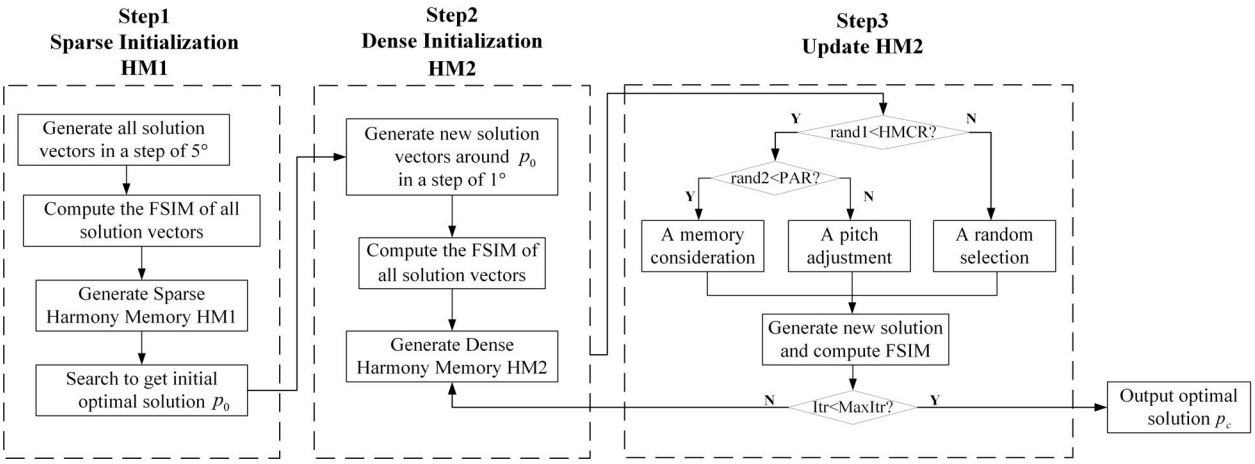

FIGURE 6. Algorithm flow chart.

FIGURE 7. All-sky polarized skylight pattern imaging device.

zenith angle. The curve in Fig.5 (a) is an approximately periodic curve of one cycle of Fig.4, and repeatedly appears according to the curve trend of Fig.5 (b). Based on the above analysis, we can draw a conclusion that the further away from the real solar position is, the lower the similarity is between the two ∞ characteristic images.

At the same time, we find that there are many minimal points on the curve in Fig.4. If the harmony memory is generated by random initialization, it is easy to fall into the locally optimum during the search process, which results in large errors. Therefore, this paper improves the harmony algorithm as follows.

First, sparse search is performed on the zenith angle and azimuth in a step of 5°, and all solution vectors (θ_i, φ_i) within the effective range are generated into the initial harmony memory HM1. By calculating negative FSIM index of all solution vectors, we can find the solution vector $p_0 = (\theta_0, \varphi_0)$ corresponding to the minimum value as the initial result.

Then the dense search will be performed around the initially determined solution vector $p_0 = (\theta_0, \varphi_0)$, with $\theta_1 \in [\theta_0 - 5°, \theta_0 + 5°]$ and $\varphi_1 \in [\varphi_0 - 5°, \varphi_0 + 5°]$ as the dense

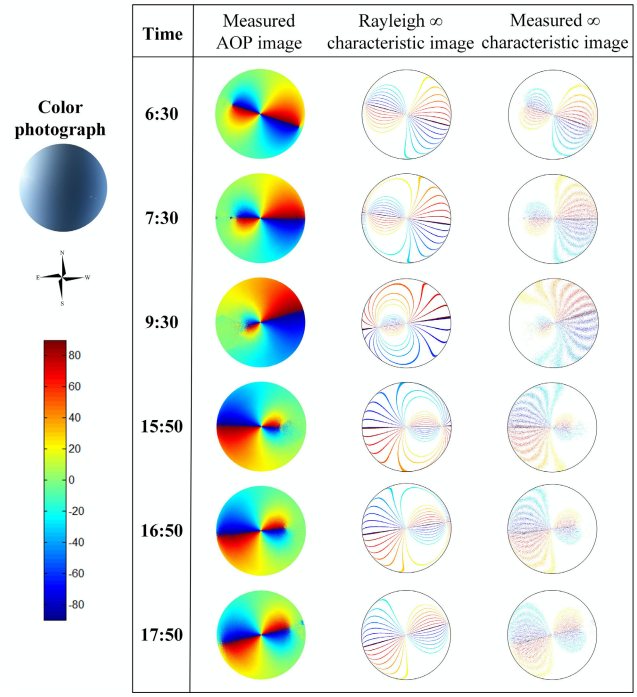

FIGURE 8. AOP images and ∞ characteristic images comparison at several moments under sunny weather.

search range, and the harmony memory HM2 will be generated in a step of 1°, respectively, and the maximum number of iterations is set to 1000. The overall algorithm flow chart is shown in Fig.6.

IV. EXPERIMENT AND DISCUSSION

In order to verify the effectiveness of the algorithm in this paper, we set up an all-sky polarized skylight pattern imaging device as shown in Fig.7. The fisheye lens uses Sigma8mmF/3.5 and the focal length is 8mm. The measurement error of linear polarization degree is less than 1.6%, and the measurement error of polarization angle is less than ±0.32° [26]. During the experiment, in order to

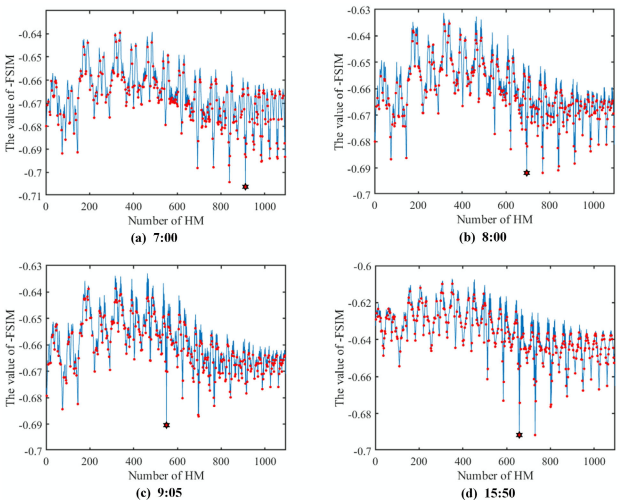

FIGURE 9. Experimental results of algorithm step 1 at 7:00, 8:00, 9:00 and 15:50.

be consistent with the coordinate system in Fig.1, the main axis of the device always points to the geographic north, and the camera is always kept horizontal. With this device, we obtain three polarized images of the sky at 0°, 60°, and 120° simultaneously, and the corresponding AOP images are calculated by the Stokes formula.

We performed many sets of tests under sunny and cloudy weather to verify the performance of the method in this paper.

A. EXPERIMENTAL RESULTS AND DISCUSSION UNDER SUNNY WEATHER

First, we performed a full-day experiment on May 23, 2019 under sunny weather. Fig.8 shows the AOP images and ∞ characteristic images comparison at several moments under sunny weather.

In Fig.8, the Rayleigh ∞ characteristic images are extracted from the simulated AOP images corresponding to the real solar positions, and the measured ∞ characteristic images are extracted from the measured AOP images. By comparing these three sets of images, we find that the AOP images under sunny days all follow the ∞ characteristic model well, and change with the change of the solar position. We perform experiments on the above measured ∞ characteristic images using the algorithm. Fig. 9 shows the experimental results of the algorithm step 1 of the AOP images at four time points, 7:00, 8:00, 9:00, and 15:50. From Fig.9, we can see that the minimum value points exist, and the minimum values are all around -0.7. Table 1 shows that the solar positions corresponding to the minimum point are the initial search results.

Table 1 shows the true solar positions, experimental results and errors at these four times.

The data in Table 1 indicate that the errors are within $\pm 5°$, which indicates that the solar position $p_0 = (\theta_0, \varphi)$ corresponding to the minimum point in Fig.9 is the result we expect. Therefore, a dense search is performed within a range of $\pm 5°$ at the initial search solar position $p_0 = (\theta_0, \varphi)$. The results of multiple experiments show that when the maximum iteration is set to 1000, the results have converged, so this paper sets the maximum iteration to 1000. The results of the dense search experiment at 7:00, 8:00, 9:00 and 15:50 are shown in Fig.10.

TABLE 1. Sparse search results under sunny weather.

Time	True values(°)		Measured values(°)		Errors(°)	
	zenith	azimuth	zenith	azimuth	zenith	azimuth
7:00	67.516	169.096	70	170	-2.484	0.904
8:00	55.915	175.531	55	180	0.915	-4.487
9:00	43.228	183.312	40	185	3.228	-1.688
15:50	50.593	1.455	50	0	0.593	1.455

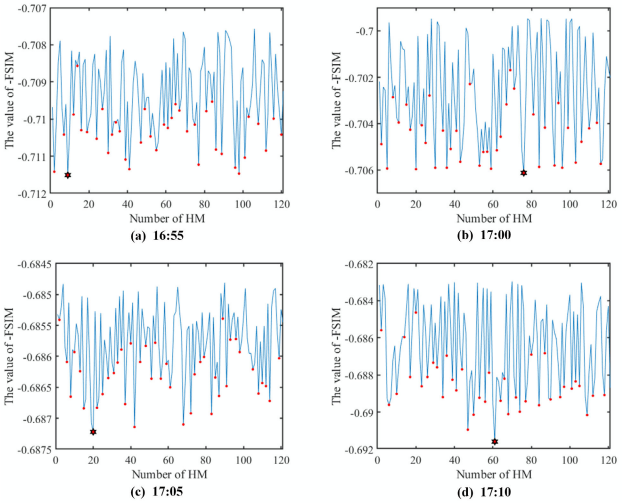

FIGURE 10. Experimental final results of algorithm at 7:00, 8:00, 9:00 and 15:50.

TABLE 2. Dense search results under sunny weather.

Time	True values(°)		Measured values(°)		Errors(°)	
	zenith	azimuth	zenith	azimuth	zenith	azimuth
7:00	67.516	169.096	67.678	169.613	-0.162	-0.517
8:00	55.915	175.531	55.720	175.952	0.291	-0.421
9:00	43.228	183.312	42.356	182.902	0.872	0.410
15:50	50.593	1.455	51.230	0.647	-0.637	0.808

From Fig.10 we can see that the minimum points exist, and their corresponding solar positions and errors with the true values are shown in Table 2. The maximum error of the zenith angle of these sets of data is 0.87°, the minimum error is 0.16°, and the maximum error of the azimuth error is 0.8°.

Fig.11 shows the error curve of the experimental results all the day. The average zenith angle error is within 0.5°, and the variance is 0.72°; the average azimuth error is within 0.4°, and the variance is 0.46°.

Outdoor experiments all the day show that our algorithm has high accuracy and can maintain long-term stability.

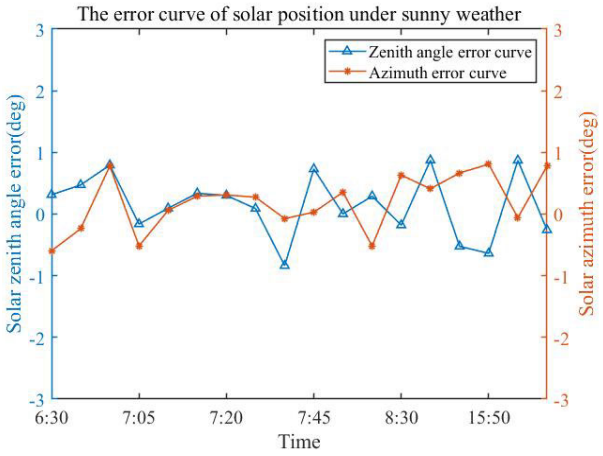

FIGURE 11. The error curve of the experimental results under the sunny weather on May 23, 2019.

B. EXPERIMENTAL RESULTS AND DISCUSSION UNDER CLOUDY WEATHER

Different weather conditions have a great influence on bionic polarized light navigation. The interference of clouds on the polarized skylight pattern makes the bionic polarized light navigation under cloudy weather a difficult research topic. [1]–[3].

Fig.12 shows the comparison between AOP images and ∞ characteristic images at several moments under cloudy weather when the ∞ characteristics are partially occluded. The experimental time was a period from 16:55 to 17:45 on June 30, 2019, with an interval of 5 minutes.

From Fig.12, we can see that the clouds has a great influence on the polarization images, which changes the distribution of AOP images partly. In this situation, the bionic polarized light navigation method that accurately calculates the polarization information of the polarized skylight pattern pixel by pixel can bring large errors. However, by comparing the theoretical ∞ characteristic image with the measured ∞ characteristic image, it is found that although the ∞ characteristic is partially destroyed, but the overall trend does not change, which illustrates the stability and effectiveness of the ∞ characteristic model.

Using the above algorithm to process the data directly under cloudy weather, large errors occur. Fig.13 shows the result of the algorithm step 1 processing of the first four sets of data.

Although there is a minimum value in Fig.13, it is not difficult to find from the data in Table 1 that the error is far greater than 5°, which indicates that the position of the sun corresponding to the minimum point in Fig.13 is not the result we expected.

Analyzing the cause of this result, we find that because the interference of the cloud layer is too large to find the optimal solution in the global scope, so we modify the algorithm step1 and design the following scheme to narrow the search range under cloudy weather. The AOP image is divided into a roulette as shown in Fig.14, and the effective range of the

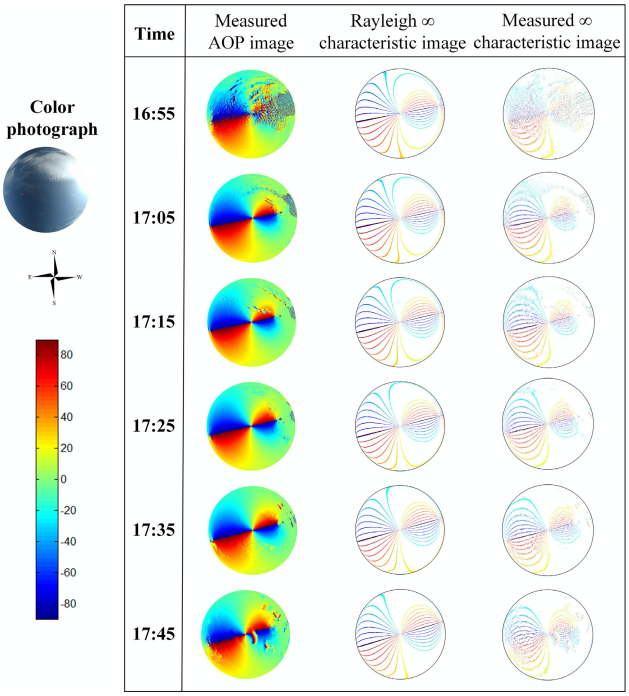

FIGURE 12. AOP images and ∞ characteristic images comparison at several moments under cloudy weather on June 30, 2019.

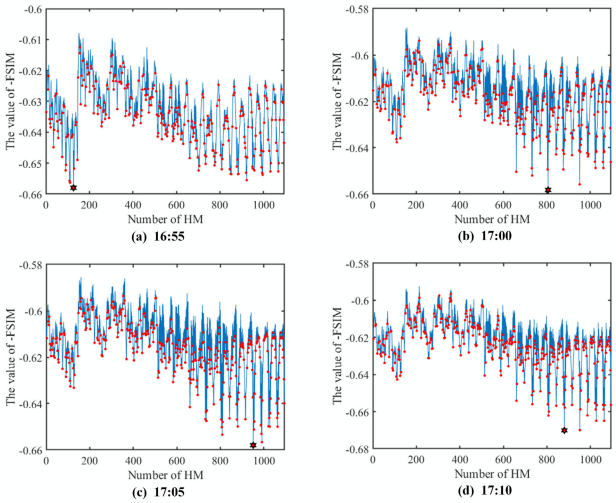

FIGURE 13. Experimental results of algorithm step 1 at 16:55, 17:00, 17:05 and 17:10.

TABLE 3. Sparse search results under cloudy weather.

Time	True values(°)		Measured values(°)		Errors(°)	
	zenith	azimuth	zenith	azimuth	zenith	azimuth
16:55	61.774	11.341	70	5	-8.226	-6.341
17:00	62.870	11.711	75	10	-12.13	1.711
17:05	63.811	12.208	85	5	-21.189	7.208
17:10	64.847	12.755	85	5	-20.153	7.755

estimated azimuth is reduced as much as possible, so that the effective search is determined in a smaller range. For example, the search range of the AOP image shown in Fig.14 can be set to [120°, 180°], and then the dense search is started from step 2 of the algorithm in this paper.

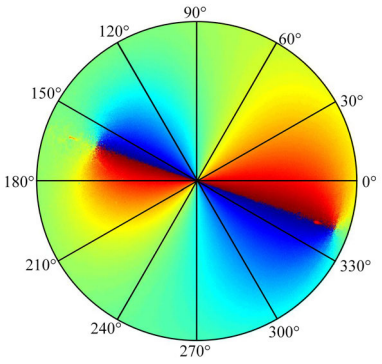

FIGURE 14. Narrow the effective search to a smaller range.

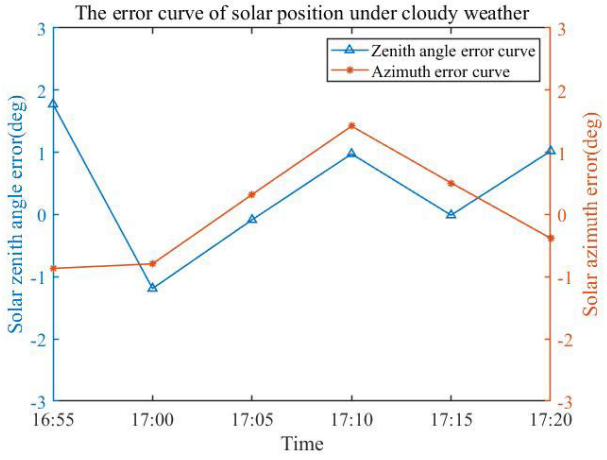

FIGURE 15. The error curve of the experimental results under the cloudy weather on June 30, 2019.

The results of processing all experimental data in cloudy weather are shown in Fig.15. The average zenith angle error is within $\pm 0.9°$ with a variance of 0.71; the average azimuth error is within $\pm 0.8°$ with a variance of 0.94. Experimental results prove the effectiveness and stability of the algorithm in this paper. If our algorithm is combined with Geomagnetic and MIMU [27], it will further improve navigation accuracy and applicability.

V. CONCLUSION

Through a large number of observational experiments, we find that the polarization angle distribution of the polarized skylight pattern presents a stable ∞ characteristic, which reflects the macroscopic distribution characteristics and changing rules of the polarized skylight pattern. Aiming at the ∞ characteristic distribution of the polarized skylight pattern, this paper proposes a method for solving the solar position based on the improved harmony search (IHS) algorithm. This paper first establishes a model of ∞ characteristic to solve the position of the sun. In this model, the feature similarity index between the measured ∞ characteristic images and the Rayleigh ∞ characteristic images generated by different solar positions as parameters is used as the judgment basis. The higher the similarity index is, the closer the solar position parameter is to the actual solar position of the measured polarization image. Then, an improved harmony search algorithm is proposed to search in the Rayleigh ∞ characteristic images database. Two initializations of the harmony memory are designed to improve the search efficiency. Finally, we can obtain the Rayleigh ∞ characteristic image with the highest feature similarity index. The corresponding solution vector is the optimal solar position. This paper validates our method on the measured polarization images under sunny and cloudy weather. The experimental results under sunny weather show that the average error of the solar azimuth angle is within 0.4°, and the average error of the solar zenith angle is within 0.5°. Under cloudy weather, when the ∞ characteristic is partially obscured, the experimental results show that the average error of the solar azimuth angle is within 0.8°, and the average error of the solar zenith angle is within 0.9°. In summary, we perform experiments with the algorithm under different weather, and the experimental results verify the stability of the ∞ characteristic model and the effectiveness of the HIS algorithm.

REFERENCES

[1] G. Horváth and D. Varju, *Polarized Light in Animal Vision-Polarization Patterns in Nature*. Berlin, Germany: Springer, 2003.
[2] B. Suhai and G. Horváth, "How well does the Rayleigh model describe the E-vector distribution of skylight in clear and cloudy conditions? A full-sky polarimetric study," *J. Opt. Soc. Amer. A, Opt. Image Sci.*, vol. 21, no. 9, pp. 1669–1676, Sep. 2004.
[3] G. P. Konnen and D. G. Stork, "Polarized light in nature," *Phys. Today* vol. 40, no. 5, p. 95, 1987.
[4] K. L. Coulson, *Polarization and Intensity of Light in the Atmosphere*, 1st ed. Hampton, VA, USA: Deepak, 1988.
[5] J. Gao and Z. G. Fan, *Bionic Polarized Light Navigation Method*. Beijing, China, 2014, pp. 101–120.
[6] M. Hamaoui, "Polarized skylight navigation," *Appl. Opt.*, vol. 56, no. 3, pp. B37–B46, Jan. 2017.
[7] G. Horváth, *Polarized Light and Polarization Vision in Animal Sciences*. Berlin, Germany: Springer, 2014.
[8] R. Wehner, "Desert ant navigation: How miniature brains solve complex tasks," *J. Comparative Physiol. A, Sensory, Neural, Behav. Physiol.*, vol. 189, no. 8, pp. 579–588, Aug. 2003.
[9] C. Evangelista, P. Kraft, M. Dacke, T. Labhart, and M. V. Srinivasan, "Honeybee navigation: Critically examining the role of the polarization compass," *Phil. Trans. Roy. Soc. B, Biol. Sci.*, vol. 369, no. 1636, Feb. 2014, Art. no. 20130037.
[10] S. Greif, I. Borissov, Y. Yovel, and R. A. Holland, "A functional role of the sky's polarization pattern for orientation in the greater mouse-eared bat," *Nature Commun.*, vol. 5, no. 1, Dec. 2014, Art. no. 4488.
[11] M. R. Dennis, "A three-dimensional degree of polarization based on Rayleigh scattering," *J. Opt. Soc. Amer. A, Opt. Image Sci.*, vol. 24, no. 7, pp. 2065–2069, Jul. 2007.
[12] W. Chuan, "Research on navigation and location method based on atmospheric polarization mode," M.S. thesis, School Comput. Inf., Hefei Univ. Technol., Hefei, China 2017.
[13] H. Lu, K. Zhao, Z. You, and K. Huang, "Angle algorithm based on Hough transform for imaging polarization navigation sensor," *Opt. Express*, vol. 23, no. 6, p. 7248, Mar. 2015.
[14] H. Lu, K. Zhao, X. Wang, Z. You, and K. Huang, "Real-time imaging orientation determination system to verify imaging polarization navigation algorithm," *Sensors*, vol. 16, no. 2, p. 144, 2016.
[15] I. Pomozi, G. Horváth, and R. Wehner, "How the clear-sky angle of polarization pattern continues underneath clouds: Full-sky measurements and implications for animal orientation," *J. Experim. Biol.*, vol. 204, no.17, pp. 2933–2942, 2001.

[16] H. Zhao, W. Xu, Y. Zhang, X. Li, H. Zhang, J. Xuan, and B. Jia, "Polarization patterns under different sky conditions and a navigation method based on the symmetry of the AOP map of skylight," *Opt. Express*, vol. 26, no. 22, pp. 28589–28603, Oct. 2018.
[17] Y. Wang, J. Chu, R. Zhang, and C. Shi, "Orthogonal vector algorithm to obtain the solar vector using the single-scattering Rayleigh model," *Appl. Opt.*, vol. 57, no. 4, p. 594, Feb. 2018.
[18] G. Han, X. He, X. Hu, L. Zhang, C. Fan, J. Mao, X. Li, and X. Wu, "A polarized light compass aided place recognition system," in *Proc. 3rd IEEE Int. Conf. Robotic Comput. (IRC)*, Naples, Italy, Feb. 2019, pp. 266–270.
[19] R. Hegedüs, S. Åkesson, and G. Horváth, "Polarization patterns of thick clouds: Overcast skies have distribution of the angle of polarization similar to that of clear skies," *J. Opt. Soc. Amer. A, Opt. Image Sci.*, vol. 24, no. 8, pp. 2347–2356, Aug. 2007.
[20] R. Hegedüs, S. Åkesson, R. Wehner, and G. Horváth, "Could vikings have navigated under foggy and cloudy conditions by skylight polarization? On the atmospheric optical prerequisites of polarimetric viking navigation under foggy and cloudy skies," *Proc. Roy. Soc. A, Math., Phys. Eng. Sci.*, vol. 463, no. 2080, pp. 1081–1095, Apr. 2007.
[21] Z. Wang, "The modeling and detection research of atmospheric polarization pattern feature based on the all sky distribution characteristic," M.S.thesis, School Comput. Inf., Hefei Univ. Technol., Hefei, China 2014.
[22] M. V. Berry, M. R. Dennis, and R. L. Lee, "Polarization singularities in the clear sky," *New J. Phys.*, vol. 6, p. 162, Nov. 2004.
[23] L. Zhang, L. Zhang, X. Mou, and D. Zhang, "FSIM: A feature similarity index for image quality assessment," *IEEE Trans. Image Process.*, vol. 20, no. 8, pp. 2378–2386, Aug. 2011.
[24] Z. Woo Geem, J. Hoon Kim, and G. V. Loganathan, "A new heuristic optimization algorithm: Harmony search," *Simulation*, vol. 76, no. 2, pp. 60–68, Feb. 2001.
[25] Q.-K. Pan, P. N. Suganthan, M. F. Tasgetiren, and J. J. Liang, "A self-adaptive global best harmony search algorithm for continuous optimization problems," *Appl. Math. Comput.*, vol. 216, no. 3, pp. 830–848, Apr. 2010.
[26] J. Sun, "Real-time Measurement System for the Pattern of All Skylight Polarization," *Opto-Electron. Eng.*, vol. 43, no. 9, pp. 45–50,2016.
[27] R. He, X. Hu, L. Zhang, X. He, and G. Han, "A combination orientation compass based on the information of polarized skylight/geomagnetic/MIMU," *IEEE Access*, vol. 8, pp. 10879–10887, 2020.

BIANBIAN LIU was born in Shanxi, China, in 1994. She received the B.S. degree from the School of Computer and Information, Hefei University of Technology, Hefei, China, in 2017, where she is currently pursuing the M.S. degree. Her current research interests include bionic polarization light navigation and outdoor test.

ZHIGUO FAN (Member, IEEE) received the B.S. degree from the Liaoning University of Science and Technology, in 2002, and the M.S. and Ph.D. degrees from the Hefei University of Technology, in 2007 and 2011, respectively. He is currently an Associate Professor with the Hefei University of Technology. His main research interests include polarized optical detection and polarized light navigation.

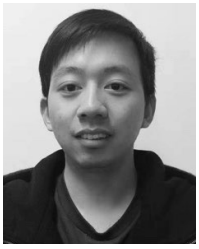

XIANQIU WANG was born in Anhui, China, in 1995. He received the B.S. degree from the School of Electronic and Information engineering, Hebei University, Baoding, China, in 2018. He is currently pursuing the M.S. degree with the Hefei University of Technology, Hefei, China. His current research interests include bionic polarization light navigation and outdoor test.